IEEE Access
Multidisciplinary | Rapid Review | Open Access Journal

Received 22 September 2022, accepted 5 October 2022, date of publication 19 October 2022, date of current version 15 November 2022.

Digital Object Identifier 10.1109/ACCESS.2022.3215491

RESEARCH ARTICLE

Dynamic Characteristic of Conductor After Ice-Shedding and Simulation Analysis of the Tension Insulator String

LV ZHONGBIN[1], XIAOHUI LIU[2], BO ZHANG[1], TAO YAGUANG[1], FANGYU LI[3], LI QING[1], AND BO YAN[4]

[1]State Grid Henan Electric Power Research Institute, Zhengzhou 450052, China
[2]State Key Laboratory of Mountain Bridge and Tunnel Engineering, Chongqing Jiaotong University, Chongqing 400074, China
[3]School of Civil Engineering, Chongqing Jiaotong University, Chongqing 400074, China
[4]College of Aerospace Engineering, Chongqing University, Chongqing 400044, China

Corresponding author: Xiaohui Liu (cqdxlxh@126.com)

This work was supported in part by the Research Project of the State Grid Corporation of China under Grant 5200-202024142A-0-0-00.

ABSTRACT Electric power fittings are the link between conductors and transmission towers, and it is essential to improve their ability to withstand damage. To obtain the actual load of electric power fittings and study the stress of each electric power fitting under the actual load, a transmission line model of catenary-shaped and an integral model of tension insulator string are established in this paper. Then, conductors with a uniform thickness of ice coating and ice shedding process are simulated by changing density method. The results show that the maximum dynamic tension of the conductor of the isolated span transmission line is greater than the static tension of conductor icing only when the length of the ice-shedding section is small. Under any ice-shedding condition, the maximum dynamic tension of the conductor of the multi-span transmission line will be close to or greater than the static tension after conductor icing. When the form conductor tension is loaded on the tension insulator string, it can be found that the most dangerous fitting in the tension insulator string is found, and the stress analysis is carried out on the key connecting fittings, which provides a reference for the design and optimization of electric power fitting.

INDEX TERMS Transmission line, ice-shedding, electrical power fitting, finite element simulation, tension insulator string.

I. INTRODUCTION

With the rapid development of electrical science and information technology, temporary social and entertainment activities are becoming more varied and colorful, and it is more important to ensure the security operations of the transmission line. The transmission line can be generally divided into conductors, electric power fittings, and transmission towers. The spatial positions of the three are shown in Fig. 1.

In actual service, the natural environment will significantly affect the safe operation of the power grid and may cause serious disasters. In winter, the ice/snow accretion of the conductors increases the vertical load on the conductors. and the vertical load will be stored in the transmission lines in the form of potential energy. When the ice/snow falls from the conductor, this elastic potential energy will be converted into the kinetic energy of the conductor's upward motion to cause the jumping of the conductor Morgan and Swift; Kollár and Farzaneh; Meng et al. The jumping of conductors will result in the dynamic impact effects on the electric power fittings and the tower Shen et al. which affects the structural stability of the whole transmission line system. In extreme cases, ice/snow accretion or ice/snow shedding on conductors has been found to cause severe damage to conductors, electric power fittings, and towers, resulting in extensive electric power breakdown Farzaneh; Lu et al.; Klinger et al., affecting normal social life and national industrial production.

The associate editor coordinating the review of this manuscript and approving it for publication was Diego Bellan.

Many scholars who take conductors as research objects conduct scale and full-scale experiments on conductors. First, the ice accretion of the conductor is equivalent to several concentrated loads. Then, removing the concentrated loads in some way to achieve that the ice accretion falls from the conductors. The displacement and dynamic tension of the conductors after the release of ice loads are studied. Such descriptions can be found in Morgan and Swift, Meng et al., and Jamaleddine et al. Numerical models of icing and ice-shedding of the conductors have been developed. It is used to study the impact of some factors, such as span, height difference, ice thickness, the position of ice-shedding and non-synchronous ice-shedding mode, on the displacement, tension, and torsion of conductors Meng et al.; Jamaleddine et al.; Fekr and McClure; Yang et al.; Ji et al.; Dong et al.

As regards electric power fittings, the insulator and ball-eye are mainly studied. Prenleloup et al. studied the stress distribution and failure characteristics of the crimped composite insulators under bending loading by applying the numerical simulation method and the experimental method. Chen et al. studied the stress distribution at the joint of the mandrel under tensile loading utilizing the numerical simulation method. The optimal crimping conditions of the composite insulators are studied by Duriatti et al., in their article, the stress distribution of the joint of the composite insulator is simulated by ANSYS. Through the fatigue test of insulators, Wankowicz and Bielecki considered that the strength of composite insulators can be represented by the power type behavior of the fatigue characteristics and that the mandrel diameter is the main determinant of fatigue and static strength of insulators. In the article published by Xie et al., the dynamic load of the transmission line can aggravate the fatigue crack growth of the mandrel.

As regards the ball-eye, the fatigue test of the ball-eye under asymmetric load and bending load is carried out. The fatigue mechanism and characteristics of the ball-eye under different stress amplitudes are analyzed in detail Xie et al.; Compared the fatigue mechanism and characteristics of ball-eye by applying different manufacturing processes Xie et al.; It is revealed that the bending load is the main reason for the fatigue failure of the ball-eye Xie et al. In recent years, scholars have carried out experiments and numerical simulations on clevis, strain clamp, and yoke connectors of overhead transmission lines Džupon et al.; Zhu et al.; Wang et al.; Zhou et al.; Sun et al. In short, it can be found that the research of electric power fittings is limited to the analysis of the single part and that the complex transmission of load in the whole tension insulator string or suspension insulator string is ignored, which makes the stress analysis of the single electric power fittings not accurate.

The research mainly analyzes the dynamic response of transmission lines and tension insulator strings after ice-shedding. This paper is organized into six sections as follows. The ice-shedding model of cable is established and verified by the literature in section 2. The dynamic response of isolated span and multi-span transmission lines under different conditions is studied in Section 3. The dynamic response of the 550 kN tension insulator string during the process of conductor ice-shedding is solved, and the response results of the key electric power fittings are analyzed in section 4. The conclusive remarks obtained in the presented study are summarized in section 5.

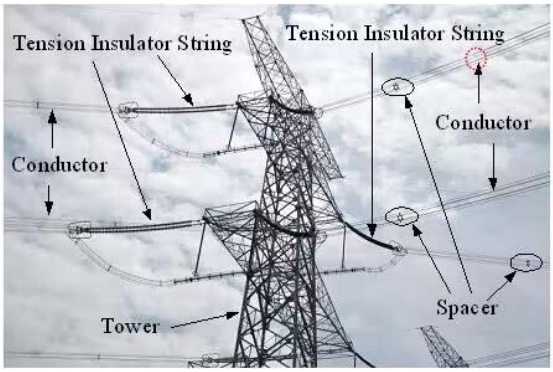

FIGURE 1. Tower line fitting location picture.

II. MODELING ICING AND ICE-SHEDDING OF CONDUCTORS

A. FE MODEL OF TRANSMISSION LINE

Because of the relatively large span and the small rigidity of the transmission line, it can be assumed as a flexible cable Ji et al.; Yan et al. Thus, for any span of the transmission lines, its geometric shape can be mathematically described by the overhead catenary equation Meng and Kong. It yields,

$$\begin{aligned} y &= \frac{\sigma_0}{\gamma}\left[\mathrm{ch}\frac{\gamma(x-a)}{\sigma_0} - \mathrm{ch}\frac{\gamma a}{\sigma_0}\right] \\ \gamma &= \frac{qg}{A} \times 10^{-3} \\ a &= \frac{l}{2} - \frac{\sigma_0}{\gamma}\mathrm{arsh}\frac{h}{\frac{2\sigma_0}{\gamma}\mathrm{sh}\frac{\gamma l}{2\sigma_0}} \end{aligned} \tag{1}$$

where, σ_0 is the horizontal stress at the lowest position of conductor sag (unit: MPa); h and l are respectively the height difference and the horizontal distance of the two supports of a single span (unit: m); q is the conductor mass per unit length (unit: kg/km); A is the area of the cross-section of the conductor (unit: mm^2); g is the acceleration of gravity, 9.8 m/s^2.

In the numerical simulation of the transmission line, the transmission line is usually modeled by the spatial two-node truss element McClure; Kollár and Farzaneh; Ji et al., and the spacer is modeled by the spatial two-node beam element Kollár and Farzaneh; Mou et al.

B. ICING AND ICE-SHEDDING MODEL

In the design of an overhead transmission line in an ice area, it is usually assumed that the ice is uniformly covered on the conductor. In numerical modeling, the conductor is divided

into two types: iced conductor and ice-shedding conductor. Icing conductors refer to the conductor with no ice falling off during the simulation process, and ice-shedding conductors refer to the conductor from which ice will be shed during the simulation process. For the iced conductor, its inertia acceleration is given as g (9.8 m/s^2), its static ice load can be modeled by increasing the density of the conductor and keeping its cross-section unchanged because the stiffness of the ice is very small concerning that of the conductor. The equivalent density ρ' Yan et al. of the iced conductor is defined as,

$$\rho' = \frac{m_1 + m_2}{A} \tag{2}$$

where, m_1 is the conductor mass per unit length (unit: kg/m); m_2 is the ice mass per unit length (unit: kg/m); A is the cross-sectional area of the conductor (unit: m^2).

During the finite-element simulation of the ice-shedding process, the density of the conductor model cannot be changed, but the inertia acceleration can. Therefore, the density of the ice-shedding conductor shall be defined as the equivalent density after the ice falls from the conductors. The density of the conductor in areas of ice shedding is regarded as equivalent to density ρ'' Yan et al.

$$\rho'' = \frac{m_1 + m_2(1-\beta)}{A} \tag{3}$$

where, β is the ice-shedding rate, and the value range of β is $0 \sim 1$.

According to the static ice load application method of the iced conductor, after the ice falls from the conductor, the inertial acceleration of the ice-shedding conductor shall be set to g (9.8 m/s^2). Besides, to ensure that the gravity of the conductor before ice shedding is equal to the "self-weight of the conductor + ice load", the inertial acceleration of the ice-shedding conductor before ice shedding is defined as equivalent inertial acceleration g'.

$$g' = \frac{m_1 + m_2}{m_1 + m_2(1-\beta)} g \tag{4}$$

The ice mass per unit length (unit: kg/m) is calculated Chen et al.,

$$m_2 = \pi \rho_i (\delta^2 + \delta d) \times 10^{-6} \tag{5}$$

where, δ is the ice thickness (unit: mm); d is the outer diameter of the conductor (unit: mm); ρi is the density of ice, 900kg/m3.

C. SIMULATION AND VALIDATION

In this sub-section, the effectiveness of the ice-shedding model proposed in Section 3.2 is validated. A single-span transmission line model as shown in Fig. 2 was used by Chen et al. to experimentally simulate the dynamic process of a transmission line after ice shedding.

In the test model, the span length is 235 m, the outer diameter of the conductor is 23.94 mm, the total cross-section

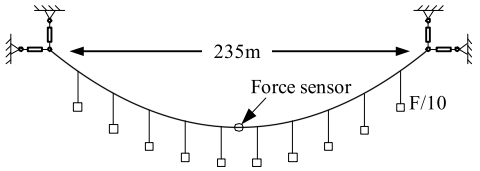

FIGURE 2. Single-span transmission line model.

area of the conductor is 338.99 mm^2, the mass of the conductor is 1.133 kg/m, the elastic modulus of the conductor is 73 GPa, and the initial tension in the conductor is 25.3 kN. It was assumed that ice with a thickness of 15 mm covered the conductor, and this load was simulated by 10 weights uniformly distributed along the conductor. A force sensor is installed to measure the tension of the conductor. To simulate ice shedding, the weights used to model the ice load were suddenly released at the same time, and the time history of the tension at the middle point of the span was recorded.

The model is established by the numerical method presented before. The physical and mechanical parameters of the conductor in the numerical model are set to be the same as those of the test model, and the geometry of the conductor is determined by the method discussed in Section 3.1. The dynamic response of the conductor after the release of the weights is numerically simulated

Fig. 3 shows the evolution of tension in the conductor at the middle position of a single-span transmission line for the cases of icing and ice shedding. When icing, the tension is maximum and constant. While ice-shedding causes the fluctuation of tension, and its amplitude gradually reduces. The simulated result by the proposed ice-shedding model in this paper is found to agree well with the experimental and simulated results in Chen et al. Therefore, it can be concluded that the ice-shedding model and the catenary-type conductor utilized in this paper are effective and reasonable.

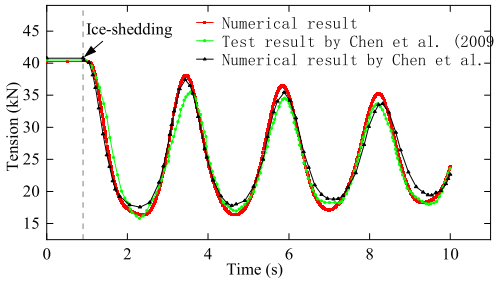

FIGURE 3. Comparison between the ice-shedding response of reference and this paper.

III. DYNAMIC CHARACTERISTIC OF CONDUCTOR AFTER ICE-SHEDDING

A. SELECTION OF TRANSMISSION LINE CHARACTERISTIC PARAMETERS

A typical finite element model of the single-span six-bundle conductor is shown in Fig. 4. The span length of the line

TABLE 1. Mechanical parameters of the conductor JL1/G2A-1250/100.

Cross-section al area (mm^2)	Diam eter (mm)	Mass per unit length (kg/m)	Young's modulus (Gpa)	Poisso n's ratio	Rated tensile strength (kN)
1350.03	47.85	4.2523	65.2	0.3	329.85

section is 500m, and the six sub-conductors are marked as C1 ∼ C6. Both ends of the bundle conductor are set to be fixed in the model. The six-bundle conductor consists of six JL1/G2A-1250/100 sub-conductors, whose mechanical parameters are shown in Table 1. The initial tension in the conductors without icing is prescribed as 20% of the rated tensile strength. The designed meteorological condition requires that the thickness of ice accretion is 20 mm without wind effect. Ice-shedding of the conductor is a very complex problem, which is usually simplified by many scholars, assuming that ice falls off the conductor by segments Meng et al.; Yang et al.; Ji et al.; Dong et al. Similarly, as for the dynamic response of the conductor in the ice-shedding process, this paper also assumes that the ice falls from the conductor by segments, and the ice-shedding rate of the conductor in the ice-shedding segments is 100%.

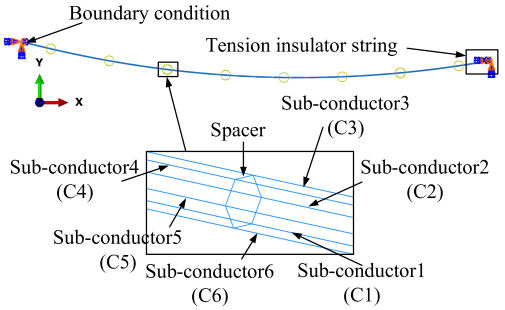

FIGURE 4. Simulation model of six bundled conductor-spacers.

B. ISOLATED SPAN TRANSMISSION LINE

To study the influence of the ice-shedding position on the tension of Isolated span transmission lines, the length of the ice-shedding section is set as 0.1 l (l is span length), and the midpoint of the ice-shedding section is 0.15 l, 0.25 l, 0.35 l, 0.45 l, 0.55 l, 0.65 l, 0.75 l, and 0.85 l respectively. Fig. 5 is the tension calculation result of the sub-conductor C1 end, and the static tension of conductor icing is 119.101 kN. The maximum dynamic tension and tension amplitude of the conductor in Fig. 5 is extracted, and the results are shown in Fig. 6. As Fig. 6 shows, the values of the maximum dynamic tension and tension amplitude correspond to the left Y-Axis and the right Y-Axis respectively (the following text is consistent). According to Fig. 5 and Fig. 6, as the ice-shedding segments of the conductor move from the end of the span to the middle of the span, the conductor tension amplitude gradually increases, and the conductor tension first decreases and then increases.

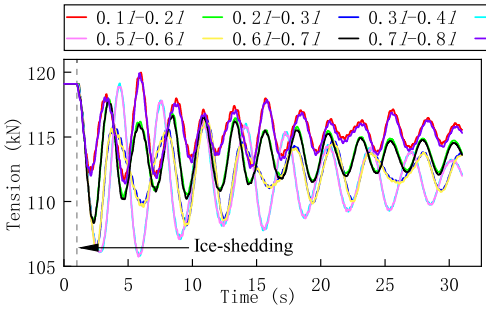

FIGURE 5. Tension time history curve of conductor.

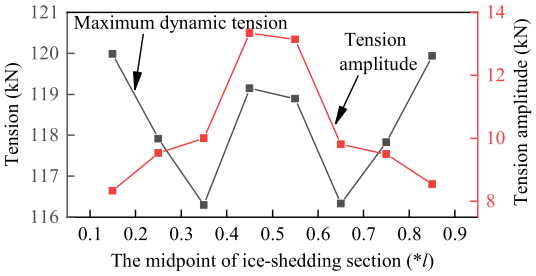

FIGURE 6. Maximum dynamic tension under different conditions at the ice-shedding position.

To determine whether the above conclusions are accidental, the midpoint of the ice-shedding section is set at 0.2 l, 0.35 l, and 0.5 l respectively, and the length of the ice-shedding section is 0.05 l, 0.1 l, 0.15 l, 0.2 l, 0.25 l, 0.35 l, and 0.4 l respectively. Similarly, the tension at the end of sub-conductor C1 is extracted to obtain Fig. 7. Obviously, the maximum dynamic tension of the conductor when the midpoint of the ice-shedding section is 0.2 l and 0.5 l is always greater than that when the midpoint of the ice-shedding section is 0.35l, which proves that the above conclusion is universal. At the same time, it can be found that when the midpoint of the ice-shedding section is in the middle of the span and the length of the ice-shedding section is short, the dynamic tension of the conductor is greater than the static tension of the conductor icing, on the contrary, the dynamic tension of the conductor is less than the static tension of the conductor icing. According to Fig. 8, the length of the ice-shedding section affects the tension amplitude of the conductor, and the tension amplitude of the conductor is in positive proportion to the length of the ice-shedding section. Based on the above research, it is suggested that the initial position of ice-shedding in a single-span transmission line should be between the end of the span and the middle of the span.

C. MULTI-SPAN TRANSMISSION LINE

Most of the actual overhead transmission lines are multi-span transmission lines. Fig. 9 shows the finite element model of the multi-span (double-span) transmission lines. The length of span1 and Span2 in Fig. 9(a) is 250m. In Fig. 9(b), the length of span1 and Span3 is 167m and that of span2 is 166m.

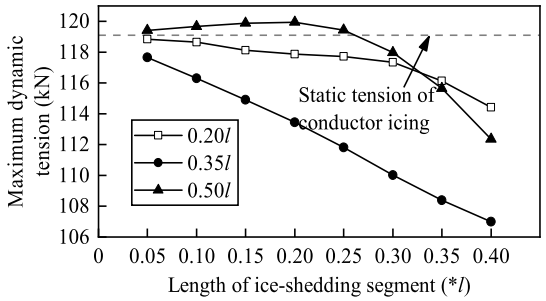

FIGURE 7. Maximum dynamic tension under different lengths of ice-shedding segment.

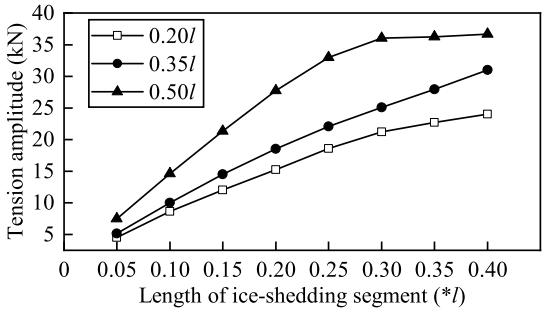

FIGURE 8. Tension amplitude under different lengths of ice-shedding segment.

Other conditions of the line are the same as those of a single-span line.

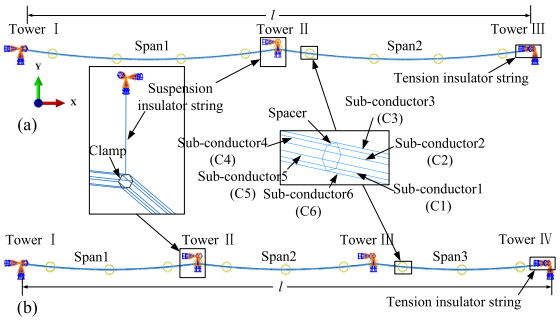

FIGURE 9. Finite element model of the multi-span transmission line. (a)Double-span, (b) Triple-span.

For the ice-shedding dynamic response of the double-span transmission line. Similarly, the tension at the end of sub conductor C1 is extracted, and the static tension of conductor icing is 105.427 kN. Set the length of the ice-shedding section of the conductor as 0.1*l* (l is the total length of Span1 and Span2), and the midpoint positions of the ice-shedding section are 0.05 *l*, 0.15 *l*, 0.25 *l*, 0.35 *l*, 0.45 *l*, 0.55 *l*, 0.65 *l*, 0.75 *l*, 0.85 *l*, and 0.95 *l* respectively. The maximum dynamic tension and amplitude results of the conductor at different positions are shown in Fig. 10. According to Fig. 10, when the ice-shedding position in Span1 moves from the end to the middle, if each span of double-span transmission lines is discussed separately, the variation law of conductor tension and tension amplitude is almost the same as that of single-span line. The midpoint of the ice-shedding section is set at 0.25 *l* of span1 and 0.75 *l* of span2. The length of the ice-shedding section is 0.05 *l*, 0.1 *l*, 0.15 *l*, 0.2 *l*, 0.25 *l*, 0.3 *l*, 0.35 *l*, 0.4 *l*, 0.45 *l* and 0.5 *l* respectively. The maximum dynamic tension and tension amplitude of the conductor are shown in Fig. 11. It can be found that the dynamic tension at the end of the conductor increases with the increase of the length of the ice-shedding section, and the ice-shedding section has little effect on the tension amplitude of the conductor in the span.

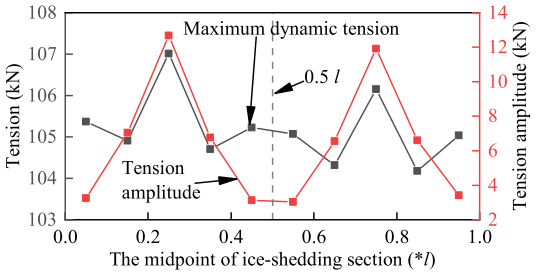

FIGURE 10. The tension of conductors in double-span lines.

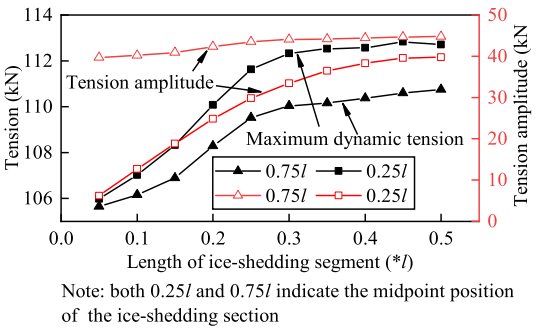

FIGURE 11. The tension of the conductor under different lengths of the ice-shedding segment in the double-span line.

For the triple-span transmission line in Fig. 9(b), the icing static tension of the conductor is 95.576 kN. The length of the ice-shedding section is set as *l* / 12. The maximum dynamic tension and tension amplitude of the conductor under different ice-shedding positions are shown in Fig. 12. It can be found that when the ice-shedding section is in the middle of each span, the dynamic tension and tension amplitude of the conductor is the largest. Similarly, to explore the influence of the length of the ice-shedding section on the stress state of the conductor, the ice-shedding area is set in the middle of each span, and the length of the ice-shedding section is *l* / 12, *l* / 6, *l* / 4, and *l* / 3 in turn. The calculation results are shown in Fig. 13. It can be found that the dynamic tension and tension amplitude of the conductor increase with the increase of the length of the ice-shedding section.

There is also a combined ice-shedding mode for multi-span transmission lines. Set all ice-shedding for each span, and the ice-shedding cases are shown in Table 2. The calculation results are shown in Fig. 14. It can be found that the dynamic

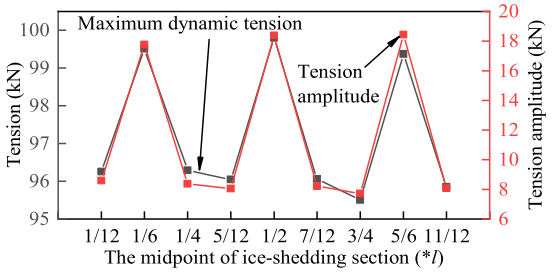

FIGURE 12. The tension of conductors in triple-span lines.

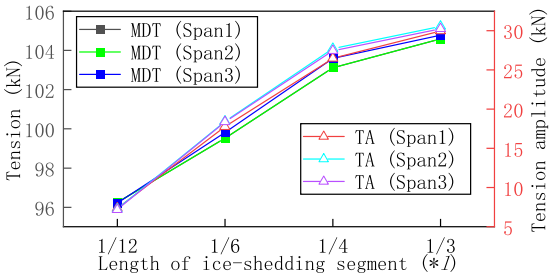

Note: MDT represents the maximum dynamic tension, TA represents the tension amplitude.

FIGURE 13. The tension of the conductor under different lengths of ice-shedding segments in the triple-span line.

TABLE 2. Test cases of ice-shedding.

Test condition	Triple-span							Double-span		
	A-1	A-2	A-3	B-1	B-2	B-3	C-1	D-1	D-2	E-1
Ice-shedding segments	Span 1	Span 2	Span 3	Span1, Span2	Span2, Span3	Span1, Span3	Span1, Span2, Span3	Span 1	Span 2	Span1, Span2

tension decreases with the increase in the number of ice-shedding spans, and the tension amplitude increases with the increase in the number of ice-shedding spans. In the multi-span transmission line, the dynamic tension and tension amplitude at the conductor end change little when the number of ice-shedding spans is the same. Considering that the electric power fittings are mostly damaged by their strength in winter, the single-span ice-shedding of the multi-span transmission line is the most dangerous.

Based on the previous research, it can be found that the influence of single-span ice-shedding on conductor tension in the multi-span transmission line is like that of the single transmission line. The difference is that the dynamic tension of the conductor after ice-shedding increases with the increase of the ice-shedding amount of the single-span of the multi-span transmission line and decreases with the increase of the ice-shedding amount of the single transmission line. In the ice-shedding process of the multi-span transmission line, the maximum dynamic tension in almost all ice-shedding modes can be close to or greater than the static tension of

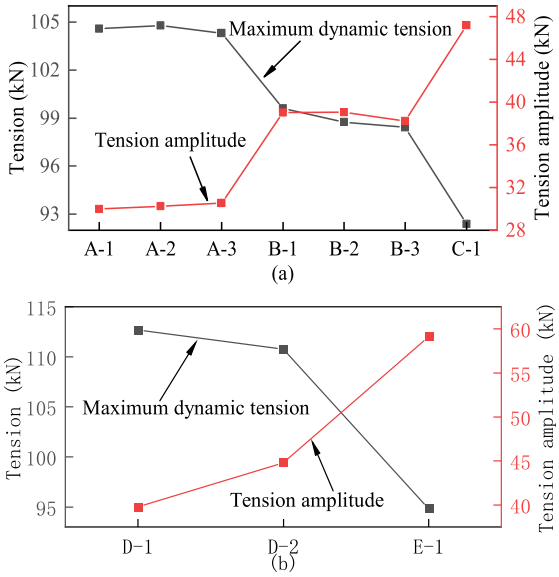

FIGURE 14. The tension of the conductor under combined ice-shedding conditions. (a) Triple-span, (b) Double-span.

conductor icing. For Isolated span transmission lines, only when the length of the ice-shedding section is small, the maximum dynamic tension of the conductor will be greater than the static tension of conductor icing. Compared with Fig. 11 and Fig. 13, for transmission lines with the same span, the increase of the span number will reduce the tension amplitude of the conductor after ice-shedding and the impact on the electric power fittings. When the total length of the multi-span transmission line and single transmission line is the same, the icing static tension of the conductor decreases with the increase of the span number. Considering that the transmission line is icing static most of the time, a single transmission line with the same length of span is more dangerous. According to Fig. 15, under the same length of the single span in the transmission line, the static tension of the conductor before ice-shedding changes little, and the dynamic tension and static tension of the conductor after ice-shedding increase with the increase of the number of spans. Therefore, the transmission line with more span numbers is more dangerous when the single span length is equal.

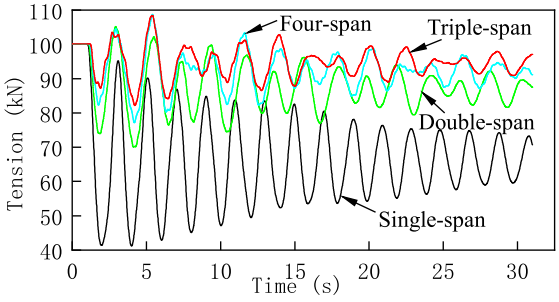

FIGURE 15. The time history curve of tension with different numbers of spans under the condition of constant sub-span length.

TABLE 3. Material properties of parts in the model.

Material types	Young's modulus (GPa)	Poisson 's ratio	Density (t/mm3)	Yield strength (MPa)	Part number
35 Steel	212	0.291	7.87× 10-9	315	1, 2, 7, 9, 12, 15 and 16
Q235-B Steel	210	0.274	7.83× 10-9	235	18
Q345 Steel	206	0.280	7.85× 10-9	345	3, 4, 5, 6, 8, 11, 13, 14 and 17
35CrMo Steel	213	0.286	7.87× 10-9	835	10

IV. FINITE ELEMENT ANALYSIS OF TENSION INSULATOR STRING

A. FE MODEL OF TENSION INSULATOR STRING

The 550kN four-tension insulator string (8N42-50100-55P) is selected as the representative in this paper. Fig. 16 shows the detailed overall calculation model of the 550kN four-tension insulator string. It should be noted that because the bolt thread has little influence on the mechanical strength of the whole structure. The bolt is simplified as a cylinder. The material types and corresponding physical parameters of the individual components of tension insulator strings are listed in Table 3. The constitutive model of the steel is a linear strengthened elastic-plastic model, and the shear modulus after yield is 1% of the elastic modulus before yield. In this calculation, the units of length, force, and stress are mm, N, and MPa, respectively.

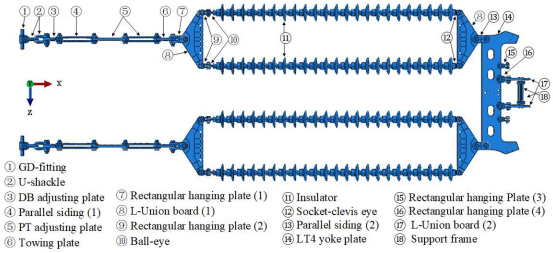

FIGURE 16. Schematic of the tension insulator string.

B. MESH AND INTERACTION

Except for the Socket-clevis eye which is modeled by the ten-node quadratic tetrahedral element (C3D10), the eight-node linear hexahedral element (C3D8R) is used for other parts of the tension insulator string.

There are 197 parts in the model, including bolts. There is a mutual rotation between parts. If the interaction between parts is defined as contact, the model calculation will not converge. Thus, the multi-body system analysis method is used to establish the interaction between parts in this paper.

ABAQUS multi-body system analysis uses connector elements in conjunction with coupling constraints to describe the constraint relationship and the relative motion between each part of the system. Defining a coupling constraint requires the specification of the reference node, the coupling nodes, and the constraint type. The coupling constraint associates the reference node with the coupling nodes. The reference nodes in the coupling constraint are then used to define appropriate connector elements between neighboring parts that enforce the desired kinematic linkage between bodies. In the whole system of tension insulator string, the two parts connected by bolts use HINGE connector elements (activate only one degree of freedom of rotation), as shown in Fig. 17(a). A U-JOINT connector element (activate only two degrees of freedom of rotation) is used between the U-shackle and the U-shackle, as shown in Fig. 17(b). Similarly, the insulator has U-JOINT connectors at both ends.

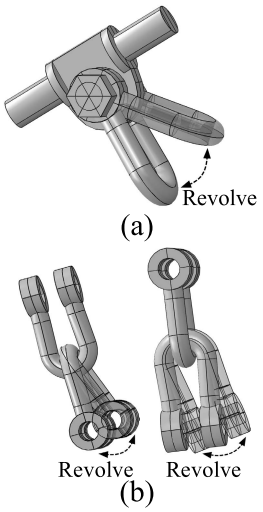

FIGURE 17. Connection type of tension insulator string. (a) HINGE. (b) U-JOINT.

In this paper, all constraint types are continuum distributing. The coupling reference points of the two connection types shown in Fig. 17 are established on the axis of rotation or contact point of the part respectively. For the U-JOINT connection type, two reference nodes couple the surfaces contacted by two parts respectively. For the HINGE connection type, one part and bolt use tie constraints, and the other part and bolt are coupled with two reference nodes respectively, as shown in Fig. 18 for details.

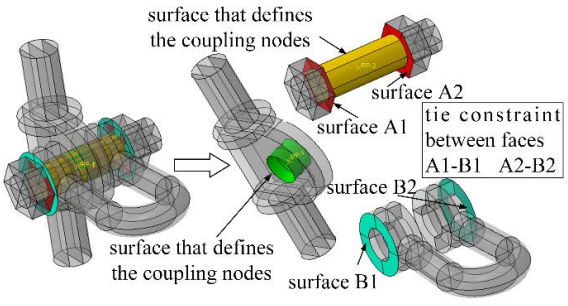

FIGURE 18. Tie and coupling diagram.

C. LOAD AND BOUNDARY CONDITIONS

According to the actual assembly of the tension insulator string and conductors, the end of the conductors is connected to part 15 and part 17 as shown in Fig 10. The specific connection positions at the tension insulator string connected to each sub-conductor are shown in Fig. 19(b). To improve the calculation efficiency, the ice-shedding model of the conductor (see Fig. 19(a) and Fig. 9) and the finite element model of the tension insulator string (see Fig.16) are separately established. Firstly, using the ice-shedding model of the conductor, the dynamic tension at the end of each sub-conductor is calculated by the finite element method. The dynamic tension components *Fx'*, *Fy'*, and *Fz'* are shown in Fig. 19(a). According to Newton's Third Law of motion action and reaction, the loads (Fx, Fy, and Fz) acting on the tension insulator string in Fig. 19(b) are equal to the dynamic tension components *Fx'*, *Fy'*, and *Fz'*. The loads (*Fx*, *Fy*, and *Fz*) are applied to the finite element model of the tension insulator string to calculate the stress distribution of the tension insulator string.

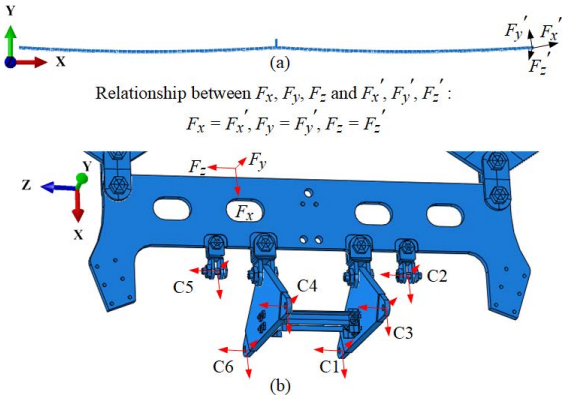

FIGURE 19. Connection position of bundled conductors in tension insulator string. (a) Schematic diagram of conductor tension component. (b) Load position and load component of tension insulator string.

Given the more common application of the multi-span transmission line in practical application, this paper takes the double-span line in Section 3 as an example to analyze the stress of tension insulator string after conductor ice-shedding. Fig. 20 shows the time history curve of the dynamic tension components *Fx'*, *Fy'*, and *Fz'* at the position of sub-conductor C1 in Fig. 19(b). Let *Fx*=*Fx'*, *Fy*=*Fy'*, and *Fz*=*Fz'*, the loads (*Fx*, *Fy*, and *Fz*) are applied on the tension insulator string. It can be found that *Fz* is almost equal to zero when the conductor bundle is ice-shedding, which is in transmission line with the actual situation that the sub-conductor has no transverse load when the bundle conductor is ice-shedding synchronously as a whole in the environment without cross wind. The value of *Fx* is always much greater than that of *Fy*, which shows that the tension insulator string is mainly affected by *Fx* in the tension in the actual ice-shedding process of the conductor. The maximum dynamic tension of the sub-conductor C1 occurs at the first wave crest after the sudden release of the ice load, as shown in Fig. 21.

According to the actual working condition of the tension insulator string, the displacement boundary conditions of GD-fittings in X, Y, and Z directions are restrained, as shown in Fig. 21.

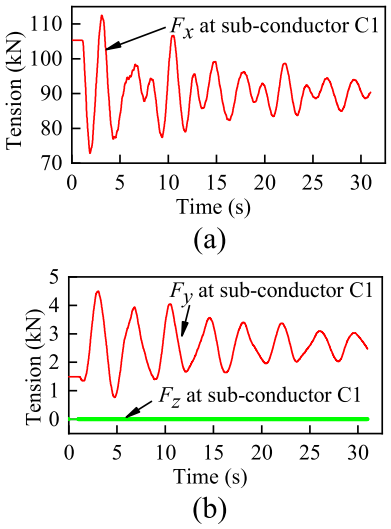

FIGURE 20. Loads of tension insulator string. (a) Fx. (b) Fy and Fz.

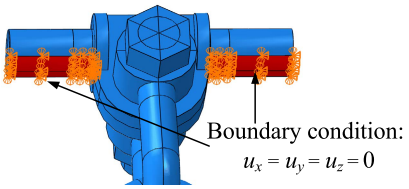

FIGURE 21. Boundary conditions of tension insulator string.

D. CALCULATION RESULTS AND DISCUSSION

The loads (*Fx*, *Fy*, and *Fz*) are applied to the tension insulator string. The stress distribution of the tension insulator string near the maximum *Fy* (Time=3.06s in Fig. 20(b)) is shown in Fig. 22. It can be found that the tension insulator string has obvious displacement in the Y direction, which is consistent with the movement under the load shown in Fig. 20. It is concluded that the two connection relations in the tension insulator string can rotate correctly.

Fig. 23 shows the comparison between the maximum stress of each fitting and the yield strength of its material under the static tension of ice coating on conductors or the dynamic tension of the conductor following ice shedding. From Fig. 23, the maximum stress of part 1 GD-fittings, part 2 U-shackle, part 11 Insulator, and part 14 LT4 yoke plate exceeds the yield strength of its material, which can be regarded as the most dangerous fittings in the tension insulator string. The maximum stress of part 17 L-Union board (2) reaches 84.7% of the yield strength of its material, which can be regarded as a secondary dangerous fitting in the tension insulator string.

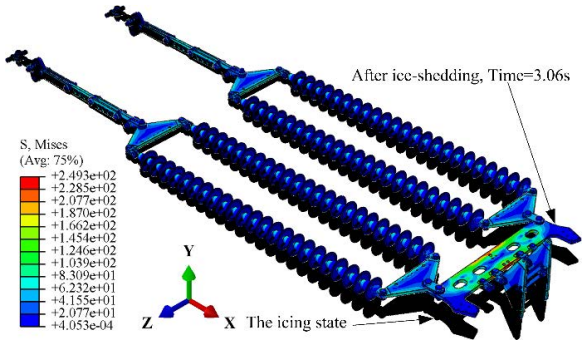

FIGURE 22. The stress distribution of tension insulator string when Time=3.06s after ice shedding of the conductor (stress unit: MPa).

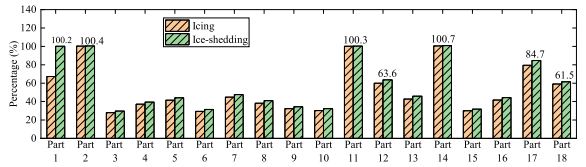

FIGURE 23. The percentage of the stress of each fitting in the yield strength of the material.

According to Fig. 23, the maximum stress of each electric power fitting (except part 1 GD-fitting) after ice-shedding is almost the same as that before ice-shedding. Comparing the stress distribution of electric power fitting at the time of maximum stress after ice-shedding with that before ice-shedding, it is found that they are almost the same. To understand the stress change of electric power fittings in more detail, the stress time history curve of dangerous points at the maximum stress and the von Mises stress distribution diagram at the maximum stress of fittings are selected as the research objects.

The stress distribution of GD- fittings before ice-shedding and stress distribution at the time of maximum stress after ice-shedding are shown in Fig. 24(a) and Fig. 24(b) respectively. It can be found that the most dangerous areas of GD-fittings before and after ice-shedding are at the connection position between the bolt and its panel. There is a sudden change of shape in this area, which makes it prone to stress concentration. The round should be used to average the stresses in this area during actual manufacturing. The stress time history curve of the integration point of the maximum stress element of GD-fittings in Fig. 24 is shown in Fig. 25. As Fig. 25 shows, the values of the stress (Point1 at GD-fitting and Point2 at GD-fitting) and force (*Fx* at sub-conductor C1) correspond to the left Y-Axis and the right Y-Axis respectively. The maximum stress of GD-fittings occurs during the period after the ice shedding of the conductor. During this period, the difference between the maximum stress and the minimum stress reaches 212MPa. The stress fluctuation of GD-fitting is more complex than the tension fluctuation of sub conductor C1. However, the overall fluctuation trend of the stress of GD-fitting is consistent with that of conductor tension.

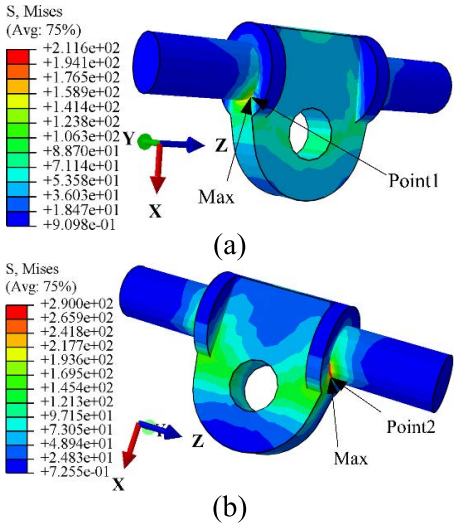

FIGURE 24. The stress distribution of GD-fittings (stress unit: MPa). (a) Before ice-shedding. (b) After ice-shedding.

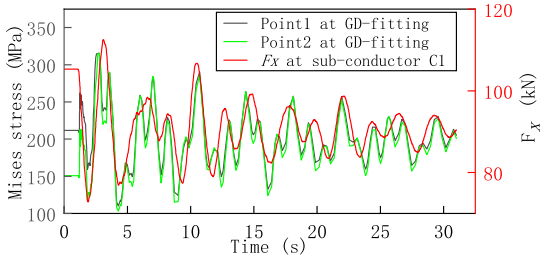

FIGURE 25. The stress time history curve of GD-fittings.

Shown in Fig. 26(a) and Fig. 26(c) are the stress distribution of the upper U-shackle and the lower U-shackle, respectively. Shown in Fig. 26(b) and Fig. 26(d) are the plastic strain distribution of the upper U-shackle and the lower U-shackle, respectively. From Fig. 26, it can be found that the maximum stress area of the U-shackle is mainly distributed in the bending part (see Fig. 26(b) for the location of this part) and the connection area between the bending part and rod part (see Fig. 26(b) for the location of this part). Looking at the plastic strain distribution of the U-shackle, it can be further clarified that the most dangerous position of the U-shackle is its bending part, which is consistent with the failure position of Fig. 27. The side shows that the model in this paper is applicability and feasibility.

Fig. 28 is the stress time-history curve of the integration point of the maximum stress element of the upper and lower U-shackle in Fig. 26. It can be found that the stress fluctuation of the upper and lower U-shackle is almost the same as the tension fluctuation of the X-axis of the conductor, indicating that the stress of the U-shackle of the tension insulator string is mainly affected by the conductor tension along the line.

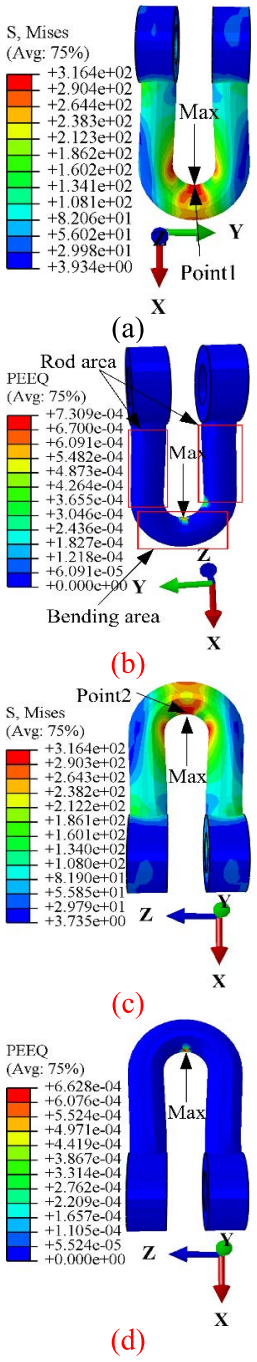

FIGURE 26. The stress and plastic strain distribution of U-shackle (stress unit: MPa). (a) Stress distribution of upper U-shackle. (b) Plastic strain distribution of upper U-shackle. (c) Stress distribution of lower U-shackle. (d) Plastic strain distribution of lower U-shackle.

Shown in Fig. 29(a) and Fig. 29(b) are stress distributions of the insulator whole view and half-cutaway View, respectively. From Fig. 29, it can be known that the maximum stress of the insulator in the whole and the half-cutaway view is distributed at the edge of the cap and the steel foot, respectively. Stress concentration happens because the edge of the cap of the insulator is not chamfered, which is not present in actual manufacturing. In the half-cutaway view

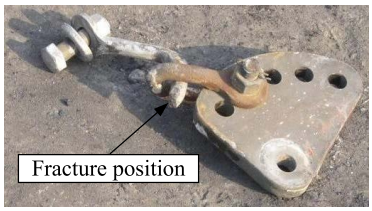

FIGURE 27. Failure case of U-shackle.

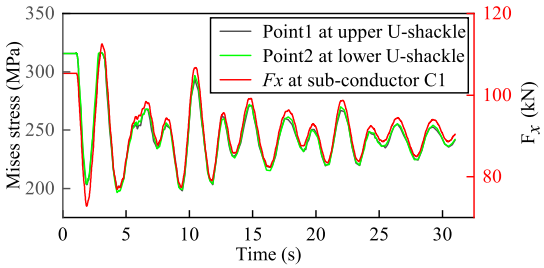

FIGURE 28. The stress time history curve of U-shackle.

(see Fig. 29(b)), the stress in the steel foot area is the largest after removing the stress concentration area. Thus, it can be inferred that in practical application, the steel foot should be the most dangerous, most easily broken, and most easily deformed area of the insulator. This inference is supported by the damage of insulators in the existing Liu et al., as shown in Fig. 30.

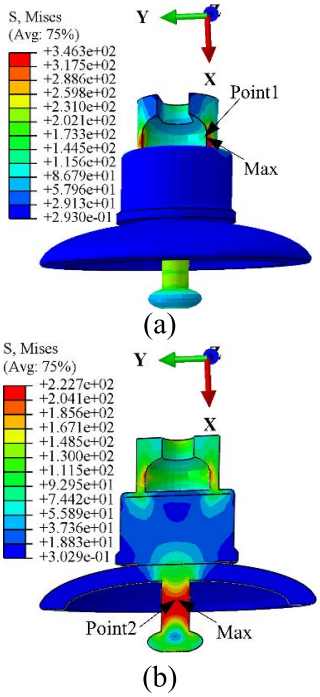

FIGURE 29. The stress distribution of insulator (stress unit: MPa). (a) Overall view of insulator. (b) Half-cutaway view of insulator.

According to the assembly picture of the tension insulator string (see Fig. 16), the six areas of the LT4 yoke plate are

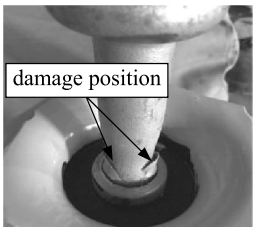

FIGURE 30. Deformation of insulator steel foot before mechanical failure.

loaded, and the load situation is complex. The research and optimization of the LT4 yoke plate can improve the structural strength and service life of the tension insulator string. Shown in Fig. 32(a) and Fig. 32(b) are the stress and plastic strain distribution of the LT4 yoke plate, respectively. The stress values near the round holes connecting part 13 parallel siding on the left and right are small, the stress values between weight loss holes 2 and 3 are small, the stress values at the upper and lower edges of the middle section are large, and there is slight plastic deformation at the lower edges of the middle section. From what has been discussed above, it can be considered to increase the thickness of the LT4 yoke plate with the high-stress area and plastic strain area, reduce the thickness of the LT4 yoke plate with less stress area, improve the strength of the LT4 yoke plate without increasing its weight, so that a load of other parts remains unchanged. In actual application, the three small holes near the point1 in Fig. 31(a) and the two locally enlarged lifting holes in Fig. 31(b) are not the direct force structure of the LT4 yoke plate, and the reason for the large stress and plastic strain is mainly due to the sudden change of the shape of the LT4 yoke plate in this area.

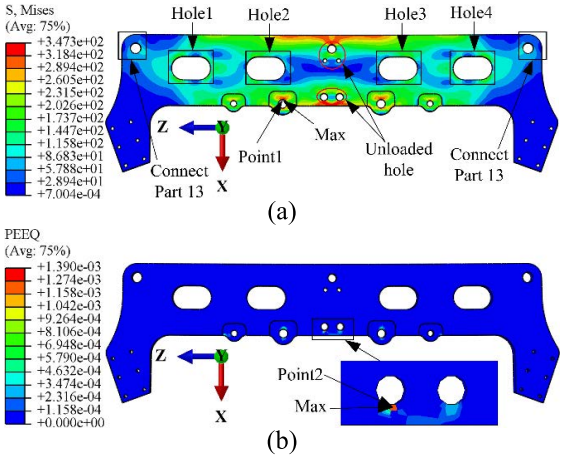

FIGURE 31. The stress and plastic strain distribution of LT4 yoke plate (stress unit: MPa). (a) Stress distribution of LT4 yoke plate. (b) Plastic strain distribution of LT4 yoke plate.

Fig. 32 shows the stress distribution of the part 17 L-Union board. The maximum stress area of part 17 L-Union board is distributed on the round hole at the position where the load is applied. From Fig. 32, the stress at the edge of the L-Union board is larger than that in other areas and the stress in the middle area is smaller. It is possible to design a hole or reduce thickness in the middle of the L-Union board to improve material utilization.

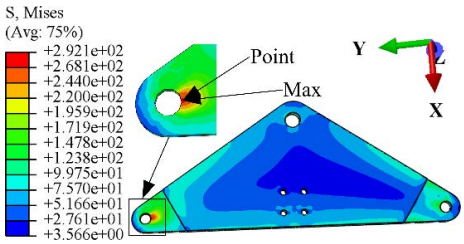

FIGURE 32. The stress distribution of part 17 L-Union board (stress unit: MPa).

According to Fig. 23, it can be found that the maximum stress of the ball-eye (part 10) accounts for 29.23% of the yield strength of its material, but its special structure and connection way (ball-cap) make it extremely vulnerable to damage in practical application. In this paper, the stress distribution of the ball-eye is shown in Fig. 33 after the tension of the conductor is applied to the tension insulator string. The maximum stress area is at the transition area between the ring and the rod, and indicates that this area is easy to damage, which is consistent with the damaged area of the ball-eye in Han et al. (see Fig. 34). It is shown that the simulation results far away from the coupling region are of the reference value and can be used for the design reference of ball-eye.

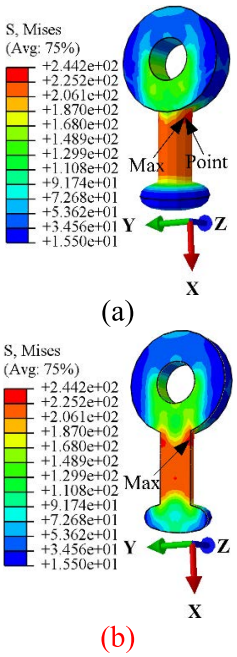

FIGURE 33. The stress distribution of Ball-eye (stress unit: MPa). (a) Overall view of ball-eye. (b) Half-cutaway view of ball-eye.

The stress time history data of the integration point of the maximum stress element or the maximum plastic strain

FIGURE 34. Fracture of ball head hanging ring Han et al.

element of the part in Fig. 29, Fig. 31, Fig. 32, and Fig. 33 are extracted, this data is shown in Fig. 35. It can be found that the waveform of the stress of the fittings is very similar to that of the conductor tension, and the time when the stress and tension reach the peak and valley is highly consistent. Combined with the analysis of the stress results of GD-fitting and U-shackle, it can be concluded that each fitting of tension insulator string (except GD-fitting) has a great correlation with the tension along the line direction of the conductor.

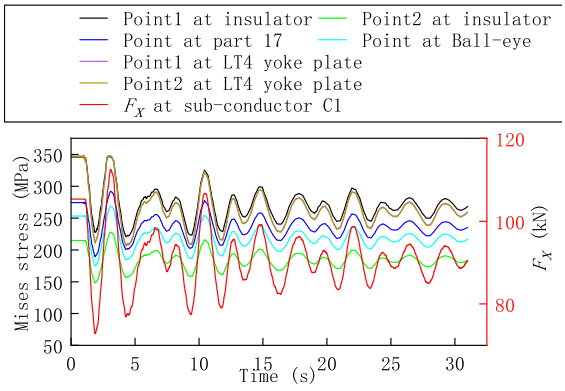

FIGURE 35. The stress time history curve of part.

Because of the above conclusions, only the maximum tension of the conductor is applied to the tension insulator string (using the static calculation method). The maximum tension of the first peak shown in Fig. 20(a) is selected as the maximum tension of the conductor. The static calculation method ignores the influence of the inertia force of the tension insulator string. Moreover, because the whole tension insulator string belongs to the tensile structure, and the direction of tensile force is consistent with the length of the tension insulator string, the acceleration in this direction is small, so the results of the static calculation method and dynamic calculation method are close. The stress results of the fittings obtained by the dynamic calculation method and the static calculation method are compared, as shown in Fig. 36- Fig. 39. It can be found that the stress results of fittings (except GD-fitting) in the two calculations methods are almost the same. The stress distribution of GD-fitting obtained by the two calculation methods is the same, the

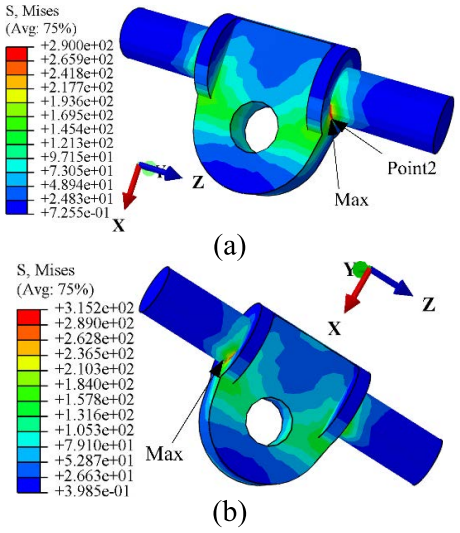

FIGURE 36. Stress calculation results of GD-fitting obtained by two calculation methods. (a) Dynamic calculation method. (b) Static calculation method.

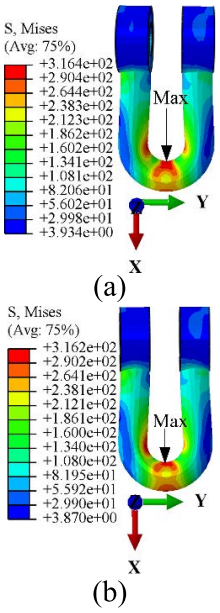

FIGURE 37. Stress calculation results of upper U-shackle obtained by two calculation methods. (a) Dynamic calculation method. (b) Static calculation method.

stress value is almost the same, and the stress of the static calculation method is greater than that of the dynamic calculation method, so the results obtained by the static calculation method are more conservative. In summary, it can be inferred that for the evaluation of the stress state of tension insulator string after conductor ice-shedding, the stress state of fittings can be calculated by selecting the maximum tension of the conductor and using the static calculation method, and the result is conservative.

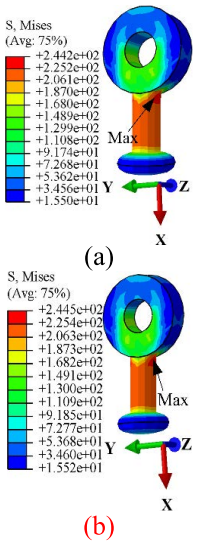

FIGURE 38. Stress calculation results of Ball-eye obtained by two calculation methods. (a) Dynamic calculation method. (b) Static calculation method.

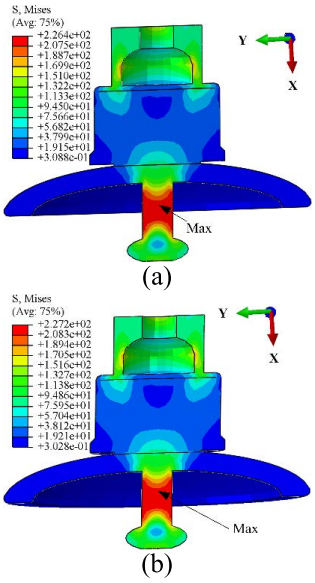

FIGURE 39. Stress calculation results of insulators obtained by two calculation methods. (a) Dynamic calculation method. (b) Static calculation method.

V. CONCLUSION

The dynamic response of the transmission line after ice-shedding is numerically simulated in this paper. The dynamic tension of the conductor was extracted and applied to the finite element model of the tension insulator string, and the stress distribution of typical fittings in the tension insulator string is analyzed, and the following conclusions are shown:

1) The maximum dynamic tension of the conductor of the isolated span transmission line is greater than the static tension of conductor icing only when the length of the ice-shedding section is small. Under any ice-shedding condition, the maximum dynamic tension of the conductor of the multi-span transmission line will be close to or greater than the static tension after conductor icing.

2) When ice-shedding is carried out in isolated transmission lines and the sub-span of multi-span transmission lines, the influence of ice-shedding position on conductor tension is similar. The maximum dynamic tension of the conductor after ice-shedding in the middle is greater than that after ice-shedding at the end.

3) The total length of the transmission line in the tension section is constant, and the conductor tension decreases with the increase of the number of sub-spans. When the length of the sub-span is constant, the conductor tension increases with the increase of the number of sub-spans.

4) GD-fittings, U-shackle, insulator, and LT4 yoke plate are the most dangerous fittings in the whole tension insulator string. The next dangerous fittings are part 17 L-Union board (2), and most of the other fittings are relatively safe. According to the actual connection form (ball-cap) and the actual failure cases, the ball-eye ring is a very easy-to-destroy electric power fitting.

5) The stress distribution of the key connection fittings shows the weak area of the fitting and guides its design improvement. The stress time history curve of electric power fitting shows that the stress change of most fittings in tension insulator string is closely related to the tension of the conductor along the line.

6) Compare the stress results of electric power fitting obtained by the dynamic calculation method and static calculation method, it can be inferred that the stress state of tension insulator string at a certain time after ice-shedding can be obtained by static calculation method, and the results are relatively conservative.

REFERENCES

[1] W. Chen, X. Dong, J. Hao, F. Yang, and X. Hu, "Analysis of the stress distribution of crimped pultruded composite rods subjected to traction," *Compos. B, Eng.*, vol. 50, pp. 362–370, Jul. 2013.
[2] Y. Chen, W. Hu, L. M. Wang, and L. Hou, "Research on ice-shedding characteristic of icing conductor," *Proc. CSEE*, vol. 29, no. 28, pp. 115–121, 2009.
[3] Y. Dong, Y. Wu, X. Rui, K. Ji, B. Liu, X. Zhan, and B. Zhao, "Research on dynamic response of bundled conductor after non-synchronous ice shedding," *J. North China Electr. Power Univ.*, vol. 45, no. 1, pp. 86–91, 2018.
[4] D. Duriatti, A. Béakou, and R. Levillain, "Optimisation of the crimping process of a metal end-fitting onto a composite rod," *Compos. Struct.*, vol. 73, no. 3, pp. 278–289, Jun. 2006.
[5] M. Džupon, L. Falat, J. Slota, and P. Hvizdoš, "Failure analysis of overhead power line yoke connector," *Eng. Failure Anal.*, vol. 33, pp. 66–74, Oct. 2013.
[6] M. Farzaneh, "Ice accretions on high–voltage conductors and insulators and related phenomena," *Philos. Trans. Roy. Soc. London A, Math., Phys. Eng. Sci.*, vol. 358, no. 1776, pp. 2971–3005, Nov. 2000.
[7] M. R. Fekr and G. McClure, "Numerical modelling of the dynamic response of ice-shedding on electrical transmission lines," *Atmos. Res.*, vol. 46, nos. 1–2, pp. 1–11, Apr. 1998.
[8] Z. Han, J. Nan, W. Cai, and Z. Wang, "Fatigue fracture failure of connection fittings on transmission line," *North China Electr. Power*, vol. 7, pp. 44–49, May 2015.
[9] A. Jamaleddine, G. McClure, J. Rousselet, and R. Beauchemin, "Simulation of ice-shedding on electrical transmission lines using Adina," *Comput. Struct.*, vol. 47, nos. 4–5, pp. 523–536, Jun. 1993.

[10] K. Ji, X. Li, B. Liu, J. Yang, P. Li, L. Zhang, X. Zhan, and B. Zhao, "Dynamic analysis of a seven-span power transmission line section following ice shedding and its suppression method," in *Proc. IEEE 8th Joint Int. Inf. Technol. Artif. Intell. Conf. (ITAIC)*, May 2019, pp. 345–349.

[11] C. Klinger, M. Mehdianpour, D. Klingbeil, D. Bettge, R. Häcker, and W. Baer, "Failure analysis on collapsed towers of overhead electrical lines in the region Münsterland (Germany) 2005," *Eng. Failure Anal.*, vol. 18, no. 7, pp. 1873–1883, Oct. 2011.

[12] L. E. Kollár and M. Farzaneh, "Vibration of bundled conductors following ice shedding," *IEEE Trans. Power Del.*, vol. 23, no. 2, pp. 1097–1104, Apr. 2008.

[13] Y. Liu, T. Yuan, S. Xu, H. Zhang, W. Wu, and Y. Zhou, "Study on stress strain characteristics of cap and pin insulator under static load," *Insulators Surge Arresters*, vol. 6, pp. 198–204, Dec. 2019.

[14] J. Lu, M. Zeng, X. Zeng, Z. Fang, and J. Yuan, "Analysis of ice-covering characteristics of China Hunan power grid," *IEEE Trans. Ind. Appl.*, vol. 51, no. 3, pp. 1997–2002, May/Jun. 2015.

[15] G. McClure and M. Lapointe, "Modeling the structural dynamic response of overhead transmission lines," *Comput. Struct.*, vol. 81, nos. 8–11, pp. 825–834, May 2003.

[16] S. Meng and W. Kong, *Design of Overhead Transmission Lines*. Beijing, China: China Electric Power Press, 2007.

[17] X. Meng, L. Wang, L. Hou, G. Fu, B. Sun, M. MacAlpine, W. Hu, and Y. Chen, "Dynamic characteristic of ice-shedding on UHV overhead transmission lines," *Cold Regions Sci. Technol.*, vol. 66, no. 1, pp. 44–52, Apr. 2011.

[18] V. T. Morgan and D. A. Swift, "Jump height of overhead-line conductors after the sudden release of ice loads," *Proc. Inst. Electr. Eng.*, vol. 111, no. 10, pp. 1736–1746, 1964.

[19] Z. Mou, B. Yan, X. Lin, G. Huang, and X. Lv, "Prediction method for galloping features of transmission lines based on FEM and machine learning," *Cold Regions Sci. Technol.*, vol. 173, May 2020, Art. no. 103031.

[20] A. Prenleloup, T. Gmür, J. Botsis, K. O. Papailiou, and K. Obrist, "Stress and failure analysis of crimped metal–composite joints used in electrical insulators subjected to bending," *Compos. A, Appl. Sci. Manuf.*, vol. 40, no. 5, pp. 644–652, May 2009.

[21] G.-H. Shen, G.-H. Yuan, B.-N. Sun, and W.-J. Lou, "Dynamic impact effects on tower-line system due to ice-shedding," *Eng. Mech.*, vol. 27, no. 5, pp. 210–217, 2010.

[22] *Abaqus 6.14 Online Documentation*, Abaqus Web, Dassault Syst. Simulia, Johnston, RI, USA, 2018.

[23] M. Sun, C. Tan, C. Zhang, C. Yang, and H. Li, "Analysis of strain clamp failure on 500 kV transmission line," *J. Mater. Sci. Chem. Eng.*, vol. 6, no. 4, pp. 47–56, 2018.

[24] Z. Q. Wang, J. Li, W. G. Yang, and Y. F. Cheng, "The finite element analysis on the compression splicing position of strain clamp in guy tower," *Appl. Mech. Mater.*, vol. 680, pp. 249–253, Oct. 2014.

[25] J. Wankowicz and J. Bielecki, "Models of the long-term mechanical strength of long rod composite insulators," *IEEE Trans. Dielectr. Electr. Insul.*, vol. 17, no. 2, pp. 360–367, Apr. 2010.

[26] Z.-S. Xie, Y. Zheng, W.-D. Shi, H.-J. Ni, Y.-Q. Zhang, Y.-P. Cao, Y. Chen, Q. Tian, and A.-N. Wang, "Investigation on the failure analysis of crimped composite insulators used in 'V' type string," *Eng. Failure Anal.*, vol. 94, pp. 274–284, Dec. 2018.

[27] Z. Xie, Y. Zheng, A. Wang, Q. Tian, Y. Chen, K. Kan, and Y. Lu, "Experimental investigation on safety and reliability of ball-eye under bending load in electrical systems," *IET Gener., Transmiss. Distrib.*, vol. 12, no. 15, pp. 3692–3698, Aug. 2018.

[28] Z. Xie, Y. Zheng, Q. Tian, A. Wang, Y. Chen, X. Mao, Y. Lu, and X. Wang, "Experimental investigation on fatigue failure characteristics of QP-16 type ball-eye under bending load," *Eng. Failure Anal.*, vol. 89, pp. 1–14, Jul. 2018.

[29] Z. Xie, Y. Zheng, A. Wang, Y. Chen, Q. Tian, and K. Kan, "Experimental study on the fatigue failure mechanism of QP-16 type ball-eye under asymmetric load," *Eng. Failure Anal.*, vol. 66, pp. 141–153, Aug. 2016.

[30] B. Yan, K. Chen, Y. Guo, M. Liang, and Q. Yuan, "Numerical simulation study on jump height of iced transmission lines after ice shedding," *IEEE Trans. Power Del.*, vol. 28, no. 1, pp. 216–225, Jan. 2013.

[31] F. Yang, J. Yang, Z. Zhang, H. Zhang, and H. Xing, "Analysis on the dynamic responses of a prototype line from iced broken conductors," *Eng. Failure Anal.*, vol. 39, pp. 108–123, Apr. 2014.

[32] Y. T. Zhou, Z. Q. Zhou, J. G. Wang, H. J. Luo, J. Zhang, and J. Y. Hu, "Study on cracking of aluminum alloy strain clamps for 500 kV transmission line," *Solid State Phenomena*, vol. 279, pp. 10–15, Aug. 2018.

[33] B. Zhu, Z. Zhu, Y. Jin, K. Wang, Y. Wang, and Y. Zhang, "Multilayered-sheet hot stamping and application in electric-power-fitting products," *Metals*, vol. 9, no. 2, p. 215, Feb. 2019.

LV ZHONGBIN was born in China. He works at the State Grid Henan Electric Power Research Institute. His research interests include security and disaster prevention and control of transmission lines.

XIAOHUI LIU was born in China. He joined the School of Civil Engineering, Chongqing Jiaotong University, in 2011, and currently a Professor. His research interests include the galloping of transmission line and dynamics of structures.

BO ZHANG was born in China. He works at the State Grid Henan Electric Power Research Institute. His research interests include security and disaster prevention and control of transmission lines.

TAO YAGUANG was born in China. He works at the State Grid Henan Electric Power Research Institute. His research interests include security and disaster prevention and control of transmission lines.

FANGYU LI was born in China. He is currently pursuing the Graduate degree with Chongqing Jiaotong University. He is also a Teacher under the supervision of Xiaohui Liu. His research interest includes galloping of transmission line.

LI QING was born in China. He works at the State Grid Henan Electric Power Research Institute. His research interests include security and disaster prevention and control of transmission lines.

BO YAN was born in China. He joined the Department of Engineering Mechanics, Chongqing University, in 1988, and currently a Professor. His research interests include solid mechanics and engineering mechanics.